

# LEFT VERSUS RIGHT HEMISPHERE DIFFERENCES IN BRAIN CONNECTIVITY: 4-TESLA HARDI TRACTOGRAPHY IN 569 TWINS

Madelaine Daianu<sup>1</sup>, Neda Jahanshad<sup>1</sup>, Emily L. Dennis<sup>1</sup>, Arthur W. Toga<sup>1</sup>, Katie L. McMahon<sup>2</sup>,  
Greig I. de Zubicaray<sup>3</sup>, Nicholas G. Martin<sup>4</sup>, Margaret J. Wright<sup>2,4</sup>, Ian B. Hickie<sup>5</sup>, Paul M. Thompson<sup>1</sup>

<sup>1</sup>Laboratory of Neuro Imaging, Department of Neurology, UCLA School of Medicine, Los Angeles, CA  
<sup>2</sup>Centre for Advanced Imaging, and <sup>3</sup>School of Psychology, University of Queensland, Brisbane, Australia

<sup>4</sup>Queensland Institute of Medical Research, Brisbane, Australia

<sup>5</sup>University of Sydney, Brain and Mind Research Institute, Australia

## ABSTRACT

Diffusion imaging can map anatomical connectivity in the living brain, offering new insights into fundamental questions such as how the left and right brain hemispheres differ. Anatomical brain asymmetries are related to speech and language abilities, but less is known about left/right hemisphere differences in brain wiring. To assess this, we scanned 457 young adults (age 23.4±2.0 SD years) and 112 adolescents (age 12-16) with 4-Tesla 105-gradient high-angular resolution diffusion imaging. We extracted fiber tracts throughout the brain with a Hough transform method. A 70x70 connectivity matrix was created, for each subject, based on the proportion of fibers intersecting 70 cortical regions. We identified significant differences in the proportions of fibers intersecting left and right hemisphere cortical regions. The degree of asymmetry in the connectivity matrices varied with age, as did the asymmetry in network topology measures such as the small-world effect.

**Index terms** – tractography, high angular resolution diffusion imaging (HARDI), small-world effect, connectome, laterality

## 1. INTRODUCTION

Diffusion MRI, and its extensions such as high angular diffusion imaging (HARDI), can be used to infer patterns of anatomical connectivity in the living brain [10]. Connectivity studies are now being extended to even larger populations, offering ever-increasing power to identify characteristic patterns of brain wiring in psychiatric and neurological disorders [6]. Surprisingly, many fundamental questions are still unanswered, such as whether the left and right brain hemispheres differ in connectivity. By contrast, morphometric brain asymmetry has been intensively studied [3].

Graph theory [10] is a powerful branch of mathematics that is increasingly applied to study how neural networks are organized. Several network topology measures have identified highly connected hubs in the brain [3]. Its anatomical and functional connections are organized as “small-world” networks and are highly modular [3]. Signs of network efficiency - such as a high clustering coefficient and short average path length - are related to intellectual function in high-density resting state EEG [7]. Full-scale IQ is also related to small-world properties in networks derived from diffusion tensor tractography [9]. Network connectivity measures may therefore offer insights into efficient information transfer in the brain [9].

Morphometric asymmetries are widely recognized for Sylvian fissure morphology and the volumes of language-related cortices such as the *planum temporale* [14]. Given these known asymmetries, which may also influence neural connectivity, we set out to use HARDI in a large cohort to find areas with left/right hemisphere differences in fiber density. We also aimed to identify

left/right differences in global network properties, such as clustering coefficient, characteristic path lengths and nodal strength. Some models of Alzheimer’s disease suggest that the hemispheres may degenerate at different rates due to differences in network connectivity [13], but data on this question has been lacking.

To address this, we scanned 569 subjects (112 adolescents and 457 young adults) with HARDI and extracted tracts throughout the brain using a HARDI tractography algorithm based on the Hough transform [1]. The tractography method used orientation density functions to provide higher order models of the diffusion process, capturing fiber crossings that might be missed if a single-tensor diffusion model is assumed [6]. Connection matrices were created to represent the proportion of brain connections interconnecting 70 cortical regions of interest, defined automatically in co-registered anatomical scans. Patterns of interhemispheric (left/right) asymmetries in the connection matrices were assessed statistically.

Furthermore, we used a set of MATLAB toolbox functions (BCT; <https://sites.google.com/a/brain-connectivity-toolbox.net/>) to analyze network topology for the right and left hemispheres, separately. We also tested if brain laterality depended on age, as the gross anatomical asymmetry of the brain increases with age, well into adolescence [12].

## 2. METHODS

### 2.1. Subjects and image acquisition

We scanned 457 right-handed young adults (mean age, 23.4±2.0 SD years) and 112 right-handed adolescents (age 12-16) with 4T HARDI and standard T1-weighted structural MRI. The participants were all twins, but genetic aspects are not considered further here. MR images were collected at the Center for Magnetic Resonance (University of Queensland) with a 4-Tesla Bruker Medspec MRI scanner (Ettingen, Germany) using a transverse electromagnetic (TEM) headcoil. T1-weighted imaging used an inversion recovery rapid gradient echo sequence with parameters: TI/TR/TE=700/1500/3.35 ms, flip angle=8°, slice thickness = 0.9 mm, and a 256x256 acquisition matrix. Diffusion-weighted images were acquired using single-shot echo planar imaging with a twice-refocused spin echo sequence to reduce eddy-current induced distortions with imaging parameters: TR/TE 6090/91.7 ms, 23 cm FOV, with a 128x128 acquisition matrix. Each 3D volume consisted of 55 2-mm thick axial slices with no gap, and a 1.79x1.79 mm<sup>2</sup> in-plane resolution.

We acquired 105 images per subject: 11 with no diffusion sensitization (i.e., T2-weighted b<sub>0</sub> images) and 94 diffusion-weighted (DW) images (b = 1159 s/mm<sup>2</sup>) with gradient directions

evenly distributed on the hemisphere, for unbiased directional sampling of the diffusion propagator. Scan time was 14.2 minutes.

## 2.2. DWI preprocessing, cortical surface extraction and registration

We preprocessed the data by automatically removing non-brain tissue from each T1-weighted MRI scan, using ROBEX [5] as well as from a T2-weighted image from the DWI set, using the FSL tool “BET” (<http://fsl.fmrib.ox.ac.uk/fsl/>). T1-weighted images were linearly aligned using FSL (with 9 DOF) to a common space [9] with 1mm isotropic voxels and a 220×220×220 voxel matrix. Raw diffusion-weighted images were corrected for eddy current distortions using FSL’s “eddy\_correct” (<http://fsl.fmrib.ox.ac.uk/fsl/>). For each subject, the 11 eddy-corrected images with no diffusion sensitization were averaged, linearly aligned and resampled to a downsampled version of their corresponding T1 image (110×110×110, 2×2×2mm). Averaged  $b_0$  maps were elastically registered to the structural scan using a mutual information cost function [8] to compensate for EPI-induced susceptibility artifacts.

## 2.3. HARDI tractography

The transformation matrix from linearly aligning the mean  $b_0$  image to the T1-weighted volume was applied to each of the 94 gradient directions to properly re-orient the orientation distribution functions (ODFs). At each HARDI voxel, ODFs were computed using the normalized and dimensionless ODF estimator, derived for QBI in [13]. This approach considers the Jacobian factor  $r^2$  to compute the constant solid angle (CSA) ODF:

$$\text{in CSA-QBI } ODF(\hat{u}) \approx \frac{1}{4\pi} + \frac{1}{16\pi^2} \text{FRT} \left\{ \nabla_{\hat{u}}^2 \ln \left( -\ln \frac{S(\hat{u})}{S_0} \right) \right\}$$

Here  $S(\hat{u})$  is the diffusion signal, and  $S_0$  is the baseline image. FRT is the Funk-Radon transform and  $\nabla_{\hat{u}}^2$  is the Laplace-Beltrami operator. We used this ODF reconstruction scheme as it improves the resolution of multiple fiber orientations [13] relative to the original QBI definition [14]. With this set of ODFs, we performed HARDI tractography on the linearly aligned DWI volumes.

Tractography was performed by seeding voxels with a prior probability based on the fractional anisotropy (FA) value derived from the single-tensor model [2]. All curves passing through a seed point receive a score estimating the probability of the existence of the fiber, computed from the ODFs. A voting process provided by the Hough transform determined the best fitting curves through each point [1].

Elastic deformations obtained from the EPI distortion correction, mapping the average  $b_0$  image to the T1-weighted image, were then applied to the tract’s 3D coordinates. Fibers with fewer than 15 points were filtered out. Each subject’s dataset contained 5000-10,000 useable fibers (3D curves).

## 2.4 Left and right hemisphere matrix analysis

A 70×70 connectivity matrix was created for each subject. The elements of this matrix represented the proportion of fibers connecting all cortical regions, within and across hemispheres; the key to these 70 regions is in [6]. To avoid applying statistical analysis to unreliable or incorrectly extracted connections, any connection was considered *invalid* if it was only found in less than 95% of the subjects.

We analyzed the left and right hemispheres individually for all 569 subjects and computed several network measures (clustering coefficient, characteristic path length, directed strengths and small-world effects) for each hemisphere using the BCT. We fitted a random effects regression model to all subjects testing for differences between the left and right hemispheres and age effects

between the left and right hemisphere connectivity matrices and scalar measures of brain connectivity. Correlated samples may arise in the tractography maps as individuals in the same family are related; therefore, we used random effects regression to correctly account for kinship and group the subjects by family. A random intercept was included for each family. Hemispheric differences were assessed after covarying for any effect of age and sex at each valid matrix connection. Moreover, we computed the element-wise difference matrix between the left and right hemispheres. In this case, BCT measures can still be applied but have a different meaning; they can identify the direction of the asymmetry (i.e., L>R or R>L) for all valid connections.

## 2.5 Clustering coefficient, characteristic path length, nodal strength and small-world effect

In graph theory, a connection matrix may be compiled that describes the topology of a network and consists of nodes and edges [11]. Nodes are represented as matrix rows and columns and the edges are the matrix entries [11]. The degree of a node,  $i$ , can be derived from the connection matrix:

$$k_i = \sum_{j \in N} a_{ij}$$

Here,  $(i,j)$  represents a link between nodes  $i$  and  $j$ , while  $a_{ij}$  is the connection status between nodes  $i$  and  $j$ .

The functional contribution of a node, and its interactions with neighboring nodes, is determined by computing the network’s *clustering coefficient*. This measures the density of the interconnected neighbors of individual nodes [11]:

$$C = \frac{1}{n} \sum_{i \in N} C_i = \frac{1}{n} \sum_{i \in N} \frac{2t_i}{k_i(k_i - 1)}$$

$C_i$  is the clustering coefficient of node  $i$  ( $C_i=0$  for  $k_i<2$ ) and  $t_i$  is the number of triangles around node,  $i$ :

$$t_i = \frac{1}{2} \sum_{j,h \in N} a_{ij} a_{ih} a_{jh}$$

The ‘triangles’ around node  $i$ , are the fraction of fully connected 3-nodes, which is equivalent to the clustering coefficient [11]. The clustering coefficient was computed from the left hemisphere 35×35 matrix,  $C_L(x,y)$ , and right hemisphere 35×35 matrix,  $C_R(x,y)$ . The left and right hemisphere matrices are undirected graphs and the difference between the two is defined by the laterality matrix,  $A(x,y)=C_L(x,y)-C_R(x,y)$ . If this matrix is thresholded to retain only connections exceeding some positive laterality threshold, then it becomes a directed graph. In directed networks, such as the asymmetry matrix  $A(x,y)$ , the incoming and outgoing edges make up the indegree ( $k_i^{IN} = \sum_{j \in N} a_{ji}$ ) and outdegree ( $k_i^{OUT} = \sum_{j \in N} a_{ij}$ ) of the network. The nodal strength is the sum of all edge weights of a node [11].

The characteristic path length, where  $L_i$  is the average distance between node,  $i$ , and all other nodes, is the number of distinct edges [11] in a network.

$$L = \frac{1}{n} \sum_{i \in N} L_i = \frac{1}{n} \sum_{i \in N} \frac{\sum_{j \in N, j \neq i} d_{ij}}{n - 1}$$

The small-world effect,  $S$ , is the ratio between the clustering coefficient and the characteristic path length after both measures are normalized relative to corresponding values obtained from randomized networks [11]. A small-world effect measure significantly greater than one indicates the coexistence of a high clustering coefficient and short path length [11].

$$S = \frac{\frac{C}{C_{rand}}}{\frac{L}{L_{rand}}}$$

### 3. RESULTS

We fitted a random effects regression model to all 569 subjects testing for differences between left vs. right hemispheres (using zeros for the left hemisphere and ones for the right hemisphere) to determine any differences between the left and right hemisphere connectivity matrices and the scalar measures of brain connectivity (clustering coefficient, nodal strength, characteristic path length and small-world effect). This set-up essentially served as a paired *t*-test as the random effects model accounts for the family relatedness between the twin subjects. We first tested the difference between the left,  $C_L(x,y)$ , and right,  $C_R(x,y)$ , hemisphere connectivity matrices in all 569 subjects using random effects regression (Fig. 1). The test returned significant differences between the left and right hemispheres at almost all cortical connections (FDR critical  $p$ -value=0.043). Some of the significant differences were between cortical regions 18, *pars opercularis*, 19, *pars orbitalis*, and 20, *pars triangularis*. These regions are of note as they form part of Broca's area, which is functionally specialized for speech production in the left hemisphere, and has known morphometric asymmetries. Even so, regions with connectivity differences extended well beyond the systems most typically studied for morphometric asymmetries. These results led us to further analyze left-right differences in the scalar measures of brain connectivity.

To determine the differences between the left and right hemisphere brain connectivity measures in all 569 subjects, we ran the random effects regression as described above and found left-right differences in the clustering coefficient ( $p < 0.034$ ), characteristic path length ( $p < 2.42 \times 10^{-10}$ ) and nodal strength ( $p < 0.041$ ). The differences between the left and right hemispheres were seen in 28 cortical regions for the nodal clustering coefficient measure, 1 cortical region for the characteristic path length and 30 cortical regions for the nodal strength. Of all these, cortical region 18, the *pars opercularis*, was significant for all measures.

The Pearson correlation between the clustering coefficients of the left and right hemispheres was significant (see above) but not high: 0.21 in adolescents and 0.33 in adults. Interestingly, the characteristic path length showed much higher correlations between left and right hemispheres: 0.49 in adolescents and 0.78 in adults. The global clustering coefficient and characteristic path length jointly determine the small-world effect. For this, a global clustering coefficient was computed by taking the mean of all local clustering coefficients for each of the adolescents and adults respectively. The ratio of the global clustering coefficient to the characteristic path length for the left and high hemisphere connection matrices is the small-world effect and is shown in Figure 3.

To see if the laterality matrix,  $A(x,y)$ , depended on age, a random effects regression was run across all subjects and an FDR critical  $p$ -value of 0.017 was found. We analyzed the beta maps to determine the asymmetry shift between the left and right hemisphere. *Beta*-values (or the slope of the regression) for significant age effects are plotted element-wise in Figure 2, which was masked by the significant and thresholded  $p$ -values obtained from the random effects regression between the left and right connectivity matrices (Fig. 1). The masked *beta*-value map consisted of 235 negative values and 229 positive values showing that the right hemisphere has more fibers with age. Significant age

effects were also found when analyzing the laterality matrix between left and right hemisphere nodes. Within these connections, many (but not all) nodes were within regions with acknowledged morphometric asymmetry, such as the *pars triangularis* and *pars opercularis*.

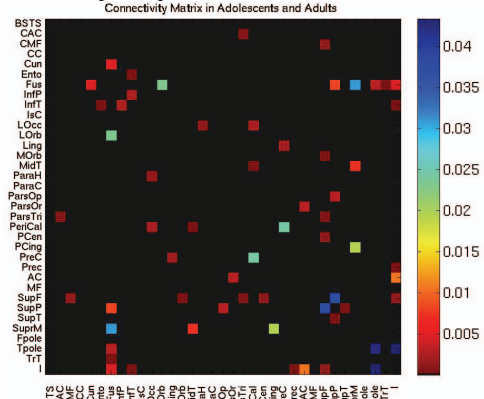


**Figure 1.** *P*-values from the random effects regression model (using zeros for the left hemisphere and ones for the right hemisphere) comparing the left,  $C_L(x,y)$ , and right,  $C_R(x,y)$ , hemisphere connectivity matrices in 112 adolescents and 457 adults (FDR critical  $p$ -value=0.0433; higher critical values denote stronger effects).

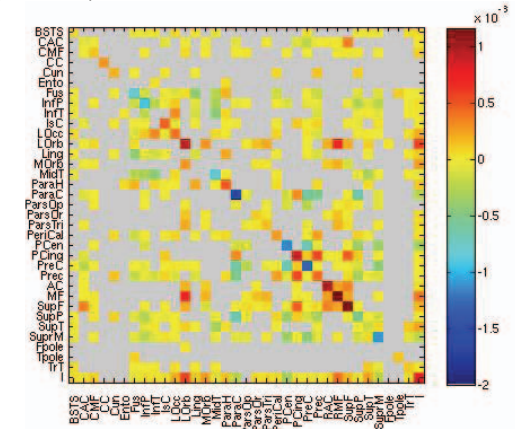


**Figure 2.** *B*-values from a random effects regression at each element of the difference matrix between the left and right connectivity matrices,  $A(x,y) = C_L(x,y) - C_R(x,y)$ , masked by the significant  $p$ -values from the random effects regression between the left and right hemispheres (Fig. 1). The gray values denote non-significant *b*-values. There are more significant negative *b*-values (235) than positive *b*-values (229), suggesting that the relative density of fibers in the right hemisphere increases with age.

1 Banks of the superior temporal sulcus	19 <i>Pars orbitalis</i>
2 Caudal anterior cingulate	20 <i>Pars triangularis</i>
3 Caudal middle frontal	21 Peri-calcarine
4 Corpus callosum	22 Postcentral
5 Cuneus	23 Posterior cingulate
6 Entorhinal	24 Pre-central
7 Fusiform	25 Precuneus
8 Inferior parietal	26 Rostral anterior cingulate
9 Inferior temporal	27 Rostral middle frontal
10 Isthmus of the cingulate	28 Superior frontal
11 Lateral occipital	29 Superior parietal
12 Lateral orbitofrontal	30 Superior temporal
13 Lingual	31 Supra-marginal
14 Medial orbitofrontal	32 Frontal pole
15 Middle temporal	33 Temporal pole
16 Parahippocampal	34 Transverse temporal
17 Paracentral	35 Insula
18 <i>Pars opercularis</i>	

**Table 1.** Index of cortical areas extracted from FreeSurfer.

Significant age effects were found for the clustering coefficient (the overall summary measure) in both the left and right hemispheres. In the left hemisphere, there were effects of age on fiber organization of the clustering coefficient measures at 17 nodes: 2, 3, 8, 9, 10, 11, 14, 16, 17, 18, 20, 22, 23, 24, 27, 29, and 31 (**Table 1**). Similarly, in the right hemisphere, the age effects were found at 14 nodes: 3, 5, 11, 12, 14, 15, 19, 20, 21, 22, 23, 26, 27 and 28.

Age differences were found in the analysis of the characteristic path length measure for the right and left hemispheres in cortical region 1. For the nodal strength measure, age effects were found at 22 nodes in the left hemisphere at regions: 1, 2, 3, 7, 8, 9, 11, 12, 14, 15, 16, 17, 18, 20, 22, 23, 24, 27, 29, 31, 34 and 35, and at 16 nodes in the right hemisphere at regions: 2, 3, 5, 9, 11, 12, 14, 19, 20, 21, 22, 23, 26, 27, 28 and 35. The banks of the superior temporal sulcus are part of this list (region 1), consistent with our prior findings of changing perisylvian asymmetry in adolescence [12].

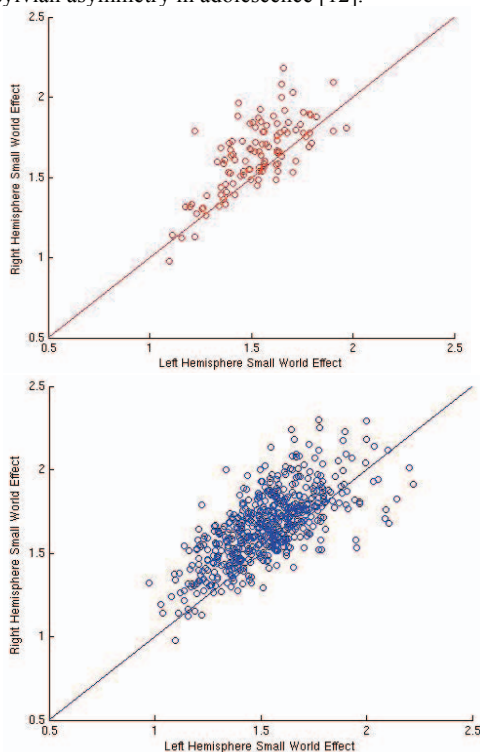


**Figure 3.** The level of “smallworldness” for the left and right hemispheres is shown for 112 adolescents (*top, red*) and 457 adults (*bottom, blue*). This measure is the ratio of the global clustering coefficient to the characteristic path length, computed from binarized connectivity matrices for the left and right hemispheres. As expected, network topology measures are highly correlated between left and right hemispheres. Small-world organization is more evident in the right hemisphere.

The directional matrix between the left and right hemisphere,  $A(x,y)$ , also showed sex differences, so sex may interact with the level of brain asymmetry (in line with prior reports of small but detectable sex differences in asymmetry and connectivity [6]). These results are omitted due to space limits.

#### 4. DISCUSSION

We used 94-direction high-angular resolution images (HARDI) in 569 individuals at 4 Tesla to trace fiber tracts throughout the brain, with orientation distribution function (ODF) based tractography. This allowed valid pursuit of the diffusion propagator where fibers mix or cross. After cortical labels were extracted automatically from co-registered surface models the interhemispheric connections were studied using statistical analysis of the binary directed connection matrices extracted from each brain.

Regions with connective asymmetry, or with significant age effects on this asymmetry, are scattered all over the brain. Regions with well-known morphometric asymmetry, such as the *pars opercularis* (a region specialized for speech in the left hemisphere) also showed asymmetric connections, but the connective asymmetry was by no means limited to well-studied temporal and parietal language areas where morphometric asymmetry is widely documented [14]. Based on the results shown by the *beta*-map (**Fig. 2**) there is an increase in the relative fiber density favoring the right hemisphere over time (or the brain becomes more asymmetric towards the right hemisphere with age). Also, the small world effect was more evident in the right hemisphere (**Fig. 3**).

#### REFERENCES:

- [1] Aganj I, *et al.* “A Hough transform global probabilistic approach to multiple-subject diffusion MRI tractography.” *Med Image Anal* 2011;15(4): 414-25.
- [2] Basser PJ and Pierpaoli C, “Microstructural and physiological features of tissues elucidated by quantitative-diffusion-tensor MRI.” *J Magn Reson B* 1996;111:209-19.
- [3] Bullmore E and Sporns O. “Complex brain networks: graph theoretical analysis of structural and functional systems.” *Nature* 2009;10:186-198.
- [4] Fischl B, *et al.* “Automatically parcellating the human cerebral cortex.” *Cereb Cortex* 2004;14:11-22.
- [5] Iglesias JE, Liu CY, Thompson PM *et al.* “Robust brain extraction across datasets and comparison with publicly available methods.” *IEEE Trans Med Imaging* 2011;30(9):1617-34.
- [6] Jahanshad N, *et al.* “Sex differences in the human connectome: 4-Tesla high angular resolution diffusion imaging (HARDI) tractography in 234 young adult twins.” *IEEE Xplore* 2011;939-943.
- [7] Langer N, *et al.* “Functional Brain Network Efficiency Predicts Intelligence.” *Human Brain Mapping* 2011 May 9. doi: 10.1002/hbm.21297.
- [8] Leow A, *et al.*, “Inverse consistent mapping in 3D deformable image registration: its construction and statistical properties.” *Inf Proc Med Imaging* 2005;19:493-503.
- [9] Li Y, *et al.* “Brain Anatomical Network and Intelligence.” *PLoS Computational Biology* 2009;5(5):1-17.
- [10] Rubinov M and Sporns O. “Complex network measures of brain connectivity: Uses and interpretations.” *NeuroImage* 2010;52:1059–1069.
- [11] Sporns O. *Networks of the Brain*. Cambridge, MA, 2011;5-31.
- [12] Sowell ER *et al.* (2002). “Mapping Sulcal Pattern Asymmetry & Local Cortical Surface Gray Matter Distribution In Vivo: Maturation in Perisylvian Cortices.” *Cereb. Cortex* 2002;12(1):17-26.
- [13] Thompson PM *et al.* “Dynamics of Gray Matter Loss in Alzheimer’s Disease.” *J. Neurosci.* 2003;23(3):994-1005.
- [14] Toga AW, Thompson PM (2003). “Mapping Brain Asymmetry.” *Nature Reviews Neurosci.* 2003;4(1):37-48.